Supporting Information

Probing the Structural Transformation and Bonding of Metal-Boride Clusters MB_3 (M = La, Ta, Re, Ir)

Xue-Lian Jiang[a], Xin-Ran Dong[a], Cong-Qiao Xu[a,*], Jun Li[a, b, c*]

[a] Department of Chemistry and Guangdong Provincial Key Laboratory of Catalytic Chemistry, Southern University of Science and Technology, Shenzhen, 518055, China.

[b] Department of Chemistry and Engineering Research Center of Advanced Rare-Earth Materials of Ministry of Education, Tsinghua University, Beijing 100084, China

[c] Fundamental Science Center of Rare Earths, Ganjiang Innovation Academy, Chinese Academy of Sciences, Ganzhou 341000, China

* Corresponding authors: xucq@sustech.edu.cn (C.Q.X.); junli@tsinghua.edu.cn (J.L.)

Geometric Structure Determination.

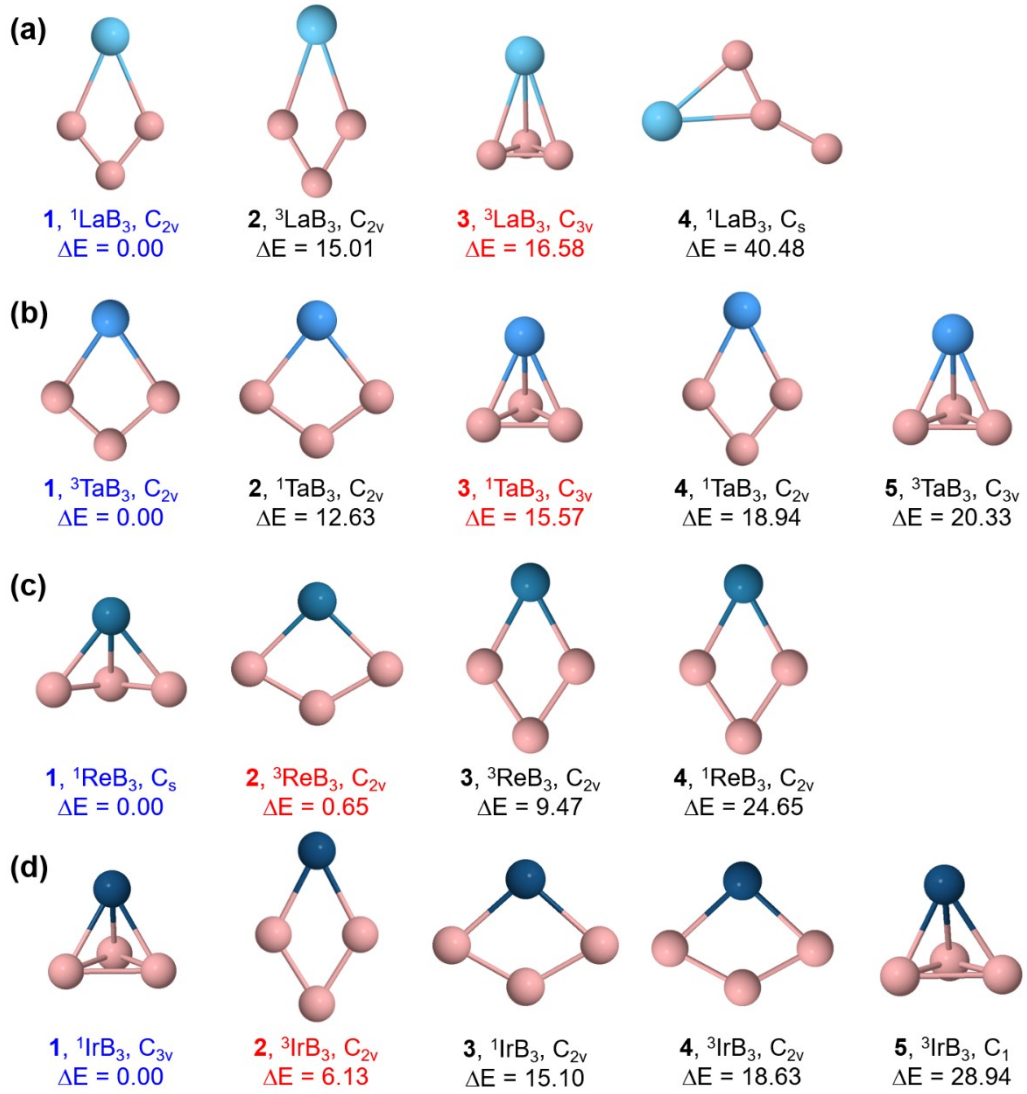

Fig. S1 The calculated lowest-energy structures and lower-lying states of neutral MB_3 (M = La, Ta, Re, Ir) clusters from the TGMin calculation at the PBE/def2-TZVP level of theory: **(a)** LaB_3, **(b)** TaB_3, **(c)** ReB_3, **(d)** IrB_3. The relative energies (ΔE) with respect to the ground state are shown in kcal/mol. The spin multiplicities are denoted as superscripts. The ground-state structures and the lower-lying states related to the 2D ↔ 3D transformation are labeled in blue and red, respectively.

Table S1. The Absolute Binding Energies (Relative to Atoms) of the Selected Isomers for MB_3 (M= La, Ta, Re, Ir) Clusters at the PBE, B3LYP, B3LYP-D3BJ and CCSD(T) Levels. The Values for the Lowest-Lying Structures are Labeled in Bold Black Font. The Isomers are Responding to the Highlighted Ones in **Fig. S1**.

PBE (Energies are in kcal/mol)			CCSD(T) (Energies are in hartree)		
M	2D	3D	M	2D	3D
La	**-384.58**	-366.39	La	**-105.5746**	-105.5412
	C_{2v}, $^1A_1$	C_{3v}, $^3A_1$		**C_{2v}, $^1A_1$**	C_{3v}, $^3A_1$
Ta	**-420.49**	-405.89	Ta	**-130.8276**	-130.8625
	C_{2v}, $^3A_2$	C_{3v}, $^1A_1$		**C_{2v}, $^3A_2$**	C_{3v}, $^1A_1$
Re	-457.84	**-459.58**	Re	-152.1553	**-152.1727**
	C_{2v}, $^3B_2$	**C_s, $^1A'$**		C_{2v}, $^3B_2$	**C_s, $^1A'$**
Ir	-452.55	**-459.37**	Ir	-178.2397	**-178.2659**
	C_{2v}, $^3B_1$	**C_{3v}, $^1A_1$**		C_{2v}, $^3B_1$	**C_{3v}, $^1A_1$**
B3LYP (Energies are in kcal/mol)			B3LYP-D3BJ (Energies are in kcal/mol)		
M	2D	3D	M	2D	3D
La	**-402.43**	-380.71	La	**-408.26**	-385.16
	C_{2v}, $^1A_1$	C_{3v}, $^3A_1$		**C_{2v}, $^1A_1$**	C_{3v}, $^3A_1$
Ta	**-466.66**	-444.59	Ta	**-472.31**	-448.91
	C_{2v}, $^3A_2$	C_{3v}, $^1A_1$		**C_{2v}, $^3A_2$**	C_{3v}, $^1A_1$
Re	-523.89	**-519.55**	Re	-529.91	**-525.56**
	C_{2v}, $^3B_2$	**C_s, $^1A'$**		C_{2v}, $^3B_2$	**C_s, $^1A'$**
Ir	-511.23	**-511.93**	Ir	-516.34	**-517.49**
	C_{2v}, $^3B_1$	**C_{3v}, $^1A_1$**		C_{2v}, $^3B_1$	**C_{3v}, $^1A_1$**

Table S2. The Bond Lengths (in Å) of the Lowest-Lying Isomers for MB_3 (M = La, Ta, Re, Ir) Clusters at the B3LYP and B3LYP-D3BJ Level. The Theoretical (Sum of Pyykkö's Covalent Atomic Radii) Single-Bond Lengths are Listed in Parentheses.

B3LYP				
Species	TM	Sym, State	TM-B/ Å	B-B/ Å
2D	La	C_{2v}, $^1A_1$	2.35(2.65)	1.53(1.70)
	Ta	C_{2v}, $^3A_2$	2.04(2.31)	1.52(1.70)
3D	Re	C_s, $^1A'$	1.89[a]/1.95(2.16)	1.65[b]/2.37(1.70)
	Ir	C_{3v}, $^1A_1$	1.87(2.07)	1.93(1.70)
B3LYP-D3BJ				
Species	TM	Sym, State	TM-B/ Å	B-B/ Å
2D	La	C_{2v}, $^1A_1$	2.36	153
	Ta	C_{2v}, $^3A_2$	2.04	1.53
3D	Re	C_s, $^1A'$	1.89[a]/1.95	1.65[a]/2.37
	Ir	C_{3v}, $^1A_1$	1.87	2.01

[a] For C_s-ReB_3, the bond length of two equivalent Re–B bonds is 1.89 Å while the other one is 1.95 Å.

[b] For C_s-ReB_3, the bond length of two equivalent B–B bonds is 1.65 Å while the other one is 2.37 Å.

Table S3. The Bond Orders (in Å) of the Lowest-Lying Isomers for MB_3 (M= La, Ta, Re, Ir) Clusters at the B3LYP Level.

Species	Cluster	Sym, State	Mayer		G-J		N-M (1)	
			TM–B	B–B	TM–B	B–B	TM-B	B–B
2D	LaB_3	C_{2v}, $^1A_1$	1.42	1.40	1.36	1.53	1.52	1.48
	TaB_3	C_{2v}, $^3A_2$	1.66	1.36	1.62	1.49	1.75	1.44
3D	ReB_3	C_s, $^1A'$	1.92[a]/1.59	0.98[b]/0.28	1.88[a]/1.39	1.18[b]/0.34	2.01[a]/1.51	1.08[b]/0.30
	IrB_3	C_{3v}, $^1A_1$	1.63	0.63	1.40	0.97	1.50	0.85

[a] For C_s-ReB_3, the bond orders of two equivalent Re–B bonds is larger while the other one is smaller.

[b] For C_s-ReB_3, the bond orders of two equivalent B–B bonds is larger while the other one is smaller.

Table S4. Computed Atomic Charges of the Lowest-Lying Isomers for MB_3 (M = La, Ta, Re, Ir) Clusters with Various Charge Partition Schemes at the B3LYP Level.

Species	Cluster	Sym, State	Mulliken		Hirshfield		VDD	
			M	B	M	B	M	B
2D	LaB_3	C_{2v}, $^1A_1$	0.35	-0.10[a]/-0.15[b]	0.68	-0.27[a]/-0.14[b]	0.77	-0.32[a]/-0.14[b]
	TaB_3	C_{2v}, $^3A_2$	0.27	-0.16[a]/0.03[b]	0.36	-0.14[a]/-0.08[b]	0.50	-0.21[a]/-0.08[b]
3D	ReB_3	C_s, $^1A'$	0.18	-0.05[a]/-0.08[b]	0.17	-0.06[a]/-0.05[b]	0.33	-0.12[a]/-0.11[b]
	IrB_3	C_{3v}, $^1A_1$	0.17	-0.06	0.08	-0.03	0.21	-0.07

[a] For the species, the atomic charges of two equivalent B atoms

[b] For the species, the atomic charges of other B atoms

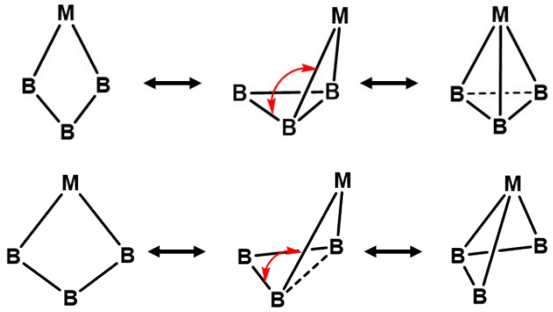

Scheme S1. Structural rearrangement between the 2D planar structure with C_{2v} symmetry and *top:* the 3D triangular pyramid geometry with C_{3v} symmetry or *bottom:* the 3D near-triangular pyramid geometry with C_s symmetry, by changing the dihedral angles (θ, in red) between metals and B_3 moieties.

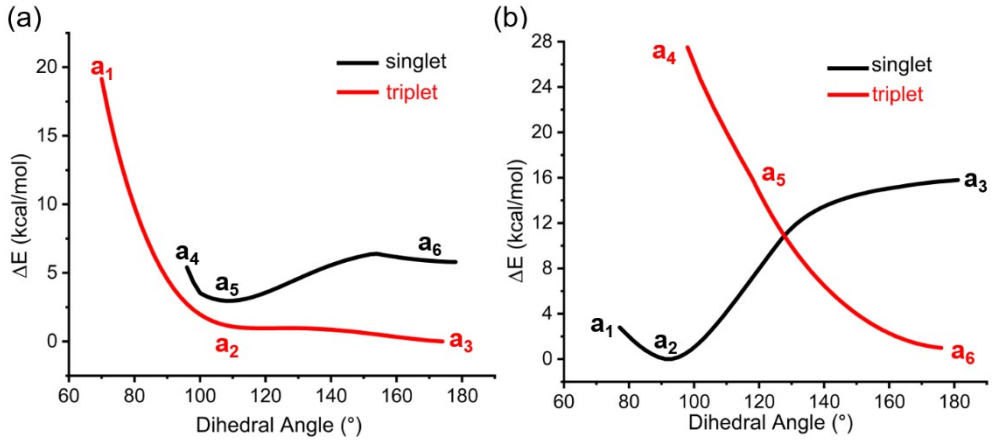

Fig. S2 Linear synchronous transit (LST) curves for structural transformation process with respect to the dihedral angles between metal atoms of **(a)** Ta, **(b)** Re and B_3 moiety at the PBE/def2-SVP level. The energy of each ground state is taken to be zero. Note: the transformation direction from left to right represents the geometric change from triangular pyramid (3D species) to planar (2D species) structure. The annotated geometries along the LST curves are provided in Fig. S3. The black line indicates the PES of the singlet state, whereas the red line depicts the PES of the triplet state.

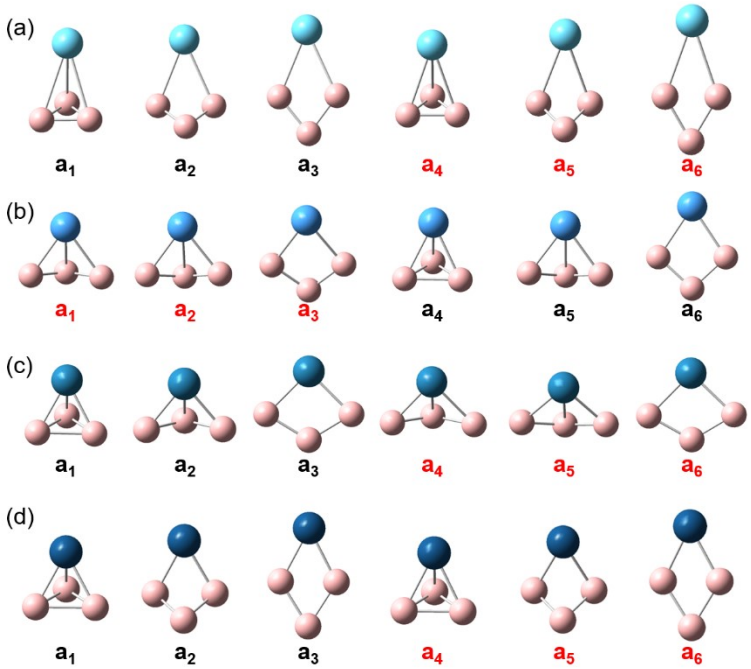

Fig. S3 The geometries along the LST curves for structural transformation process of **(a)** LaB_3, **(b)** TaB_3, **(c)** ReB_3, **(d)** IrB_3 in Fig. 2 and Fig. S2.

MO Analysis.

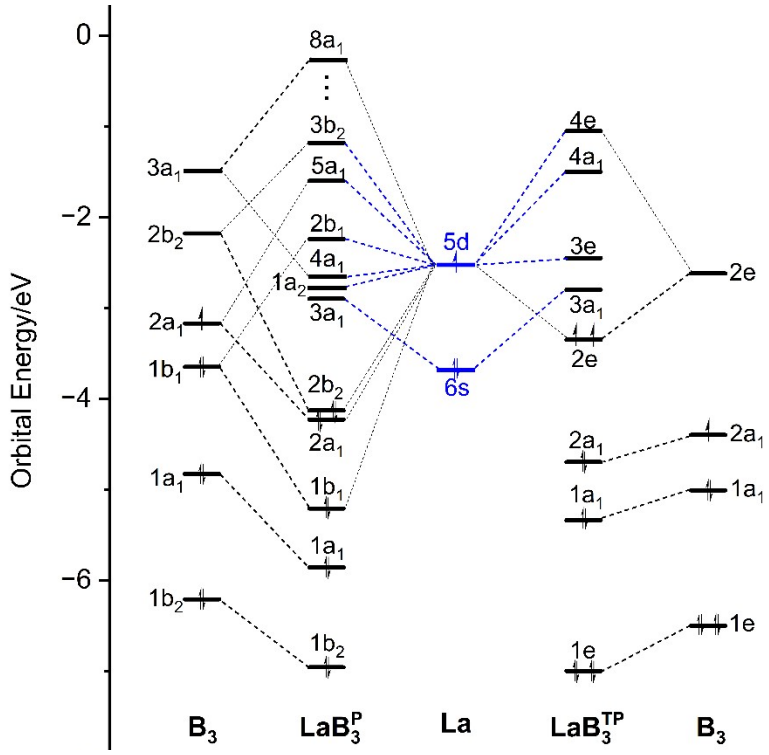

Fig. S4 Comparison of the Kohn-Sham molecular orbital energy levels between the 2D planar (*left*, C_{2v} symmetry) and 3D triangular pyramid (*right*, C_{3v} symmetry) LaB_3 isomers, using the fragments of La and B_3.

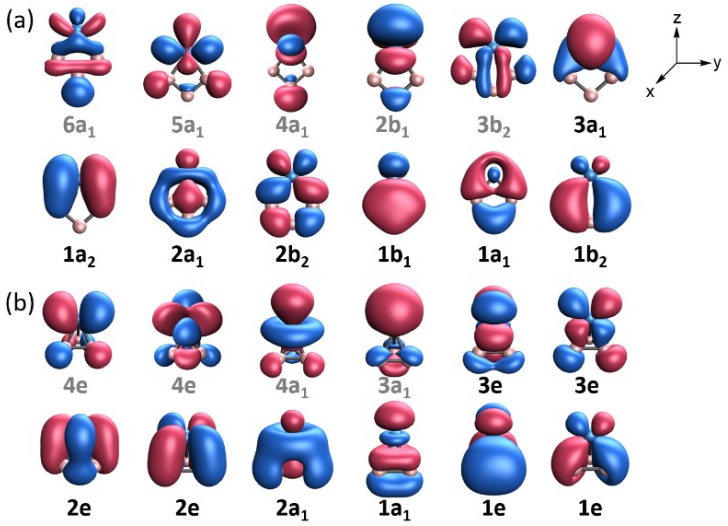

Fig. S5 Comparison of the Kohn-Sham MO contours between **(a)** 2D planar (C_{2v} symmetry) and **(b)** 3D triangular pyramid (C_{3v} symmetry) TaB_3 isomers. The occupied MOs are labeled in black and the empty orbitals in grey.

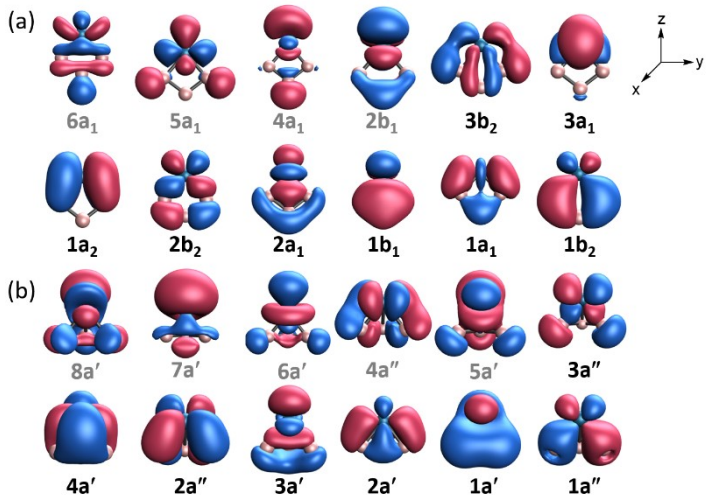

Fig. S6 Comparison of the Kohn-Sham MO contours between **(a)** 2D planar (C_{2v} symmetry) and **(b)** 3D triangular pyramid (C_{3v} symmetry) ReB_3 isomers. The occupied MOs are labeled in black and the empty orbitals in grey.

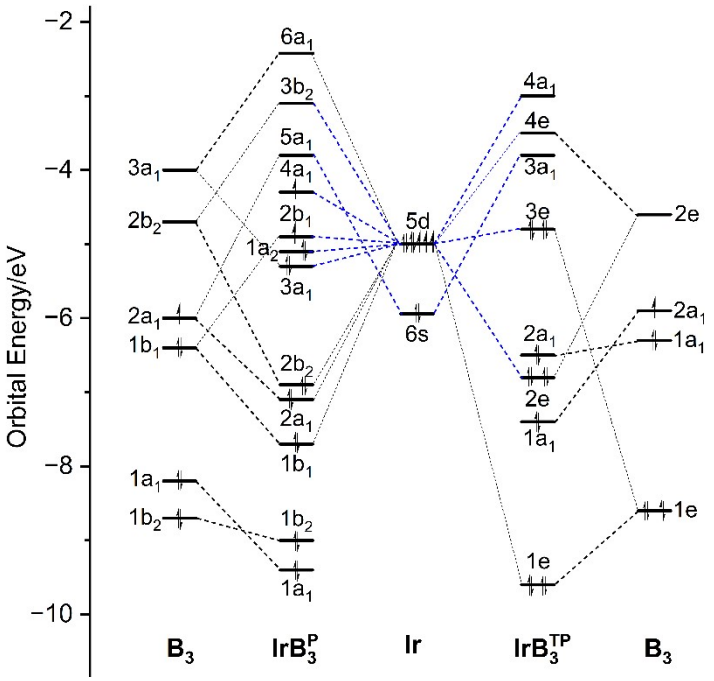

Fig. S7 Comparison of the Kohn-Sham molecular orbital energy levels between the 2D planar (*left*, C_{2v} symmetry) and 3D triangular pyramid (*right*, C_{3v} symmetry) IrB_3 isomers, using the fragments of Ir and B_3.

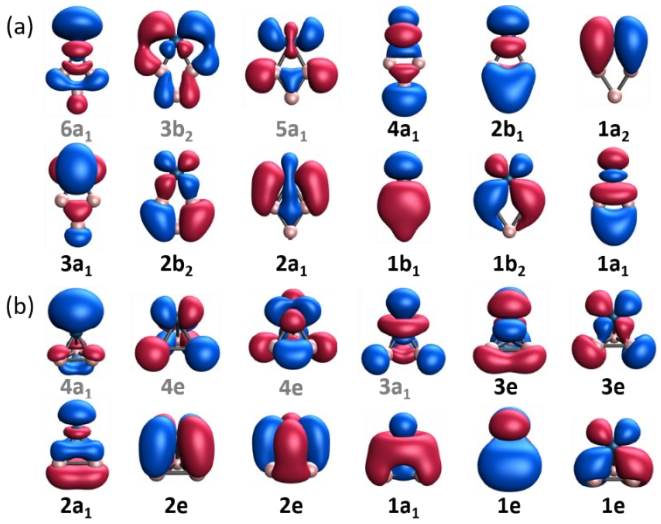

Fig. S8 Comparison of the Kohn-Sham MO contours between **(a)** 2D planar (C_{2v} symmetry) and **(b)** 3D triangular pyramid (C_{3v} symmetry) IrB_3 isomers. The occupied MOs are labeled in black and the empty orbitals in grey. The related energy levels are shown in **Fig. S3**.

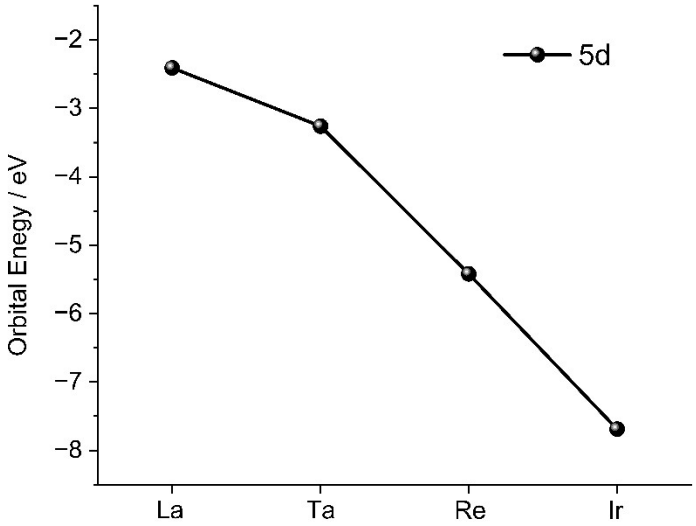

Fig. S9 The energy of the valence 5d orbitals for La-Ir at the B3LYP/TZ2P level.

Table S5. EDA results for LaB_3 and IrB_3 molecules at the B3LYP/TZP Level, with different fragmental charge repartition.

Energy term	LaB_3		IrB_3	
	$La^{3+} + B_3^{3-}$	$La^{1-} + B_3^{1+}$	$Ir^{3+} + B_3^{3-}$	$Ir^{1-} + B_3^{1+}$
ΔE_{int}	-1210.00	-381.35	-1896.42	-428.88
ΔE_{Pauli}	333.69	434.70	957.95	1208.94
ΔE_{elstat}	-1113.62	-241.72	-1617.63	-861.86
ΔE_{orb}	-430.07	-574.33	-1236.74	-775.96

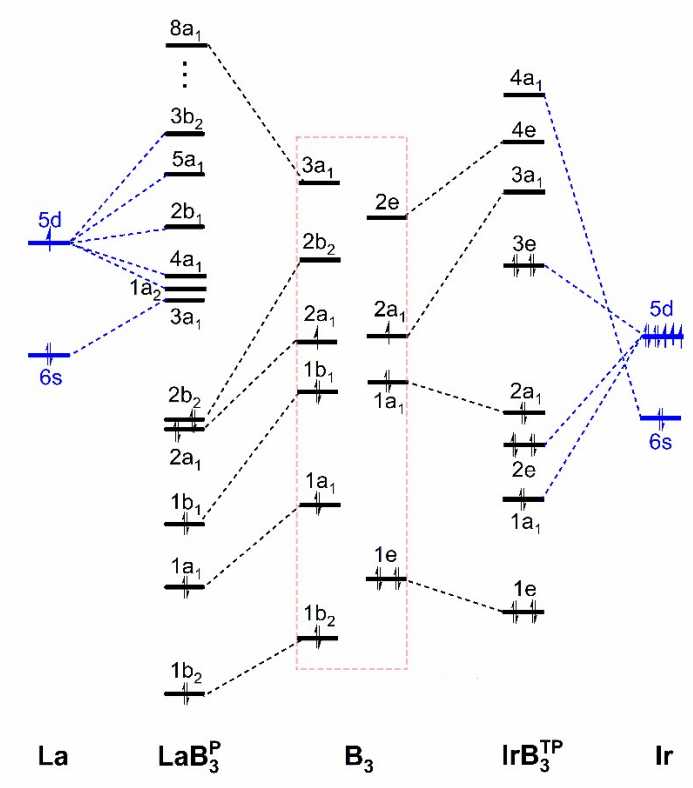

Fig. S10 Schematic MO energy-level correlation diagram of LaB_3^P and IrB_3^{TP} molecules by considering the metal and triboron fragments.

Table S6. AO Composition (in %) of the Kohn-Sham Molecular Orbitals for the Lowest-Lying Structures of MB_3 (M = La, Ir) Clusters at the B3LYP/TZ2P Level. The Labels of the MOs are Consistent with that in Fig. 3 and Fig. S4.

MO	LaB_3
$\mathbf{3b_2}$	40.9%La($5d_{yz}$) + 29.8%La(5p) + 29.3%B(2p)
$\mathbf{5a_1}$	65.6%La($5d_{x2-y2}$) + 9.6%La($5d_{z2}$) + 12.2%La(5p) + 12.6%B(2p)
$\mathbf{2b_1}$	68.4%La($5d_{xz}$) + 16.4%La(5p) + 15.2% B(2p)
$\mathbf{4a_1}$	46.9%La($5d_{z2}$) + 3.6%La($5d_{x2-y2}$) + 15.5%La(5p) + 9.2%B(2s) + 24.8%B(2p)
$\mathbf{1a_2}$	88.4%La($5d_{xy}$) + 11.6%B(2p)
$\mathbf{3a_1}$	26.8%La($5d_{x2-y2}$) + 5.3%La($5d_{z2}$) + 37.1%La(6s) + 20.0%La(5p) + 10.8%B(2p)
$\mathbf{2b_2}$	36.9%La($5d_{yz}$) + 2.0%B(2s) + 61.1%B(2p)
$\mathbf{2a_1}$	2.2%La($5d_{z2}$) + 4.9%La($5d_{x2-y2}$) + 24.0%La(6s) + 15.4%B(2s) + 53.5%B(2p)
$\mathbf{1b_1}$	21.7%La($5d_{xz}$) + 78.3%B(2p)

$1a_1$	13.9%La($5d_{z2}$) + 8.0%La(6s) + 32.9%B(2s) + 45.2%B(2p)
$1b_2$	10.5%La($5d_{yz}$) + 56.5%B(2s) + 33%B(2p)

MO	**TaB_3**
$6a_1$	33.4% Ta($5d_{z2}$) + 17.2%Ta($5d_{x2-y2}$) + 12.0% B(2s) + 37.4%B(2p)
$5a_1$	26.8% Ta($5d_{yz}$) + 8.8%Ta(6p) + 6.1%B(2s) + 58.3%B(2p)
$2b_1$	58.2%Ta($5d_{xz}$) + 16.3%Ta(6p) + 25.5%B(2p)
$4a_1$	26.4%Ta($5d_{z2}$) + 10.7%Ta($5d_{x2-y2}$) + 30.4%Ta(6p/7s) +10.2%B(2s)+ 22.3%B(2p)
$3b_2$	25.0%Ta($5d_{yz}$) + 12.2%Ta(6p) + 6.9%B(2s) + 55.9%B(2p)
$3a_1$	56.0%Ta($5d_{x2-y2}$) +3.4%Ta($5d_{z2}$) +33.3%Ta(6s) +3.2%B(2s) +4.1%B(2p)
$1a_2$	82.4%Ta($5d_{xy}$) +17.6%B(2p)
$2a_1$	28.5% Ta($5d_{z2}$) + 4.0%Ta(6s) +21.0%B(2s) + 46.5%B(2p)
$1b_1$	30.8% Ta($5d_{xz}$) + 3.1%Ta(6p) + 66.1%B(2p)
$2b_2$	33.4%Ta($5d_{yz}$) + 66.6%B(2p)
$1a_1$	4.5% Ta($5d_{x2-y2}$) + 29.5%Ta(6s) + 24.7%B(2s) + 41.3%B(2p)
$1b_2$	15.8% Ta($5d_{yz}$) + 3.1% Ta(6p) + 58.2%B(2s) + 22.9%B(2p)

MO	**ReB_3**
5a″	16.6%Re($5d_{xz}$) + 9.9% Re($5d_{yz}$) + 4.3%Re(6p) + 69.2%B(2p)
7a′	16.2%Re($5d_{z2/x2-y2}$) + 6.1% Re($5d_{xy}$) + 14.5%Re(6s) + 7.8%B(2s) +
6a′	23.9%Re($5d_{x2-y2}$) + 5.3% Re($5d_{z2}$) + 6.9%Re(6p) + 14.8%Re(7s) + 49.1%B(2p)
4a″	34.2%Re($5d_{yz}$) + 5.7%Re(6p) + 2.0%B(2s) + 58.1%B(2p)
5a′	31.0%Re($5d_{xy}$) + 5.4%Re($5d_{z2/x2-y2}$) + 22.0%B(2s) + 41.6%B(2p)
3a″	25.1%Re($5d_{xz}$) + 12.8% Re($5d_{yz}$) + 28.3%B(2s) + 33.8%B(2p)
4a′	36.5%Re($5d_{z2}$) + 22.6%Re($5d_{x2-y2}$) + 4.4%Re($5d_{xy}$) + 19.7% Re(6s) + 16.8%B(2p)
2a″	40.9%Re($5d_{yz}$) + 11.5%Re($5d_{xz}$) + 47.6%B(2p)
3a′	13.8%Re($5d_{x2-y2}$) + 6.2%Re($5d_{xy}$) + 4.7%Re(6s) + 19.5%B(2s) + 55.8%B(2p)
2a′	25.8%Re($5d_{z2}$) + 11.3%Re($5d_{xy/x2-y2}$) + 13.2%Re(6s) + 8.6%B(2s) + 41.1%%B(2p)
1a′	32.5%Re($5d_{xy}$) + 7.8%Re($5d_{z2/x2-y2}$) + 4.3%Re(6s) + 30.7%B(2s) + 24.7%B(2p)
1a″	30.7%Re($5d_{xz}$) + 44.1%B(2s) + 17.1%B(2p)

MO	**IrB_3**
4e	19.5%Ir($5d_{x2-y2/xz//xy/yz}$) + 4.1%B(2s) + 76.4%%B(2p)
$4a_1$	16.3%Ir($5d_{z2}$) + 58.2%Ir(6s) + 5.1%B(2s) + 20.4%B(2p)
$3a_1$	40.0%Ir($5d_{z2}$) + 16.1%Ir(6s) + 5.7%B(2s) + 38.2%B(2p)
3e	30.7%Ir($5d_{xz/yz}$) + 40.0%B(2s) + 29.3%B(2p)
2e	79.3%Ir($5d_{x2-y2/xy}$) + 20.7%B(2p)

$2a_1$	4.1%Ir($5d_{z2}$) + 22.5%Ir(6s) + 13.8%B(2s) + 59.6%B(2p)
$1a_1$	50.8%Ir($5d_{z2}$) + 12.6%Ir(6s) + 19.2%B(2s) + 17.4%B(2p)
1e	53.9%Ir($5d_{xz/yz}$) + 29.0%B(2s) + 17.1%B(2p)

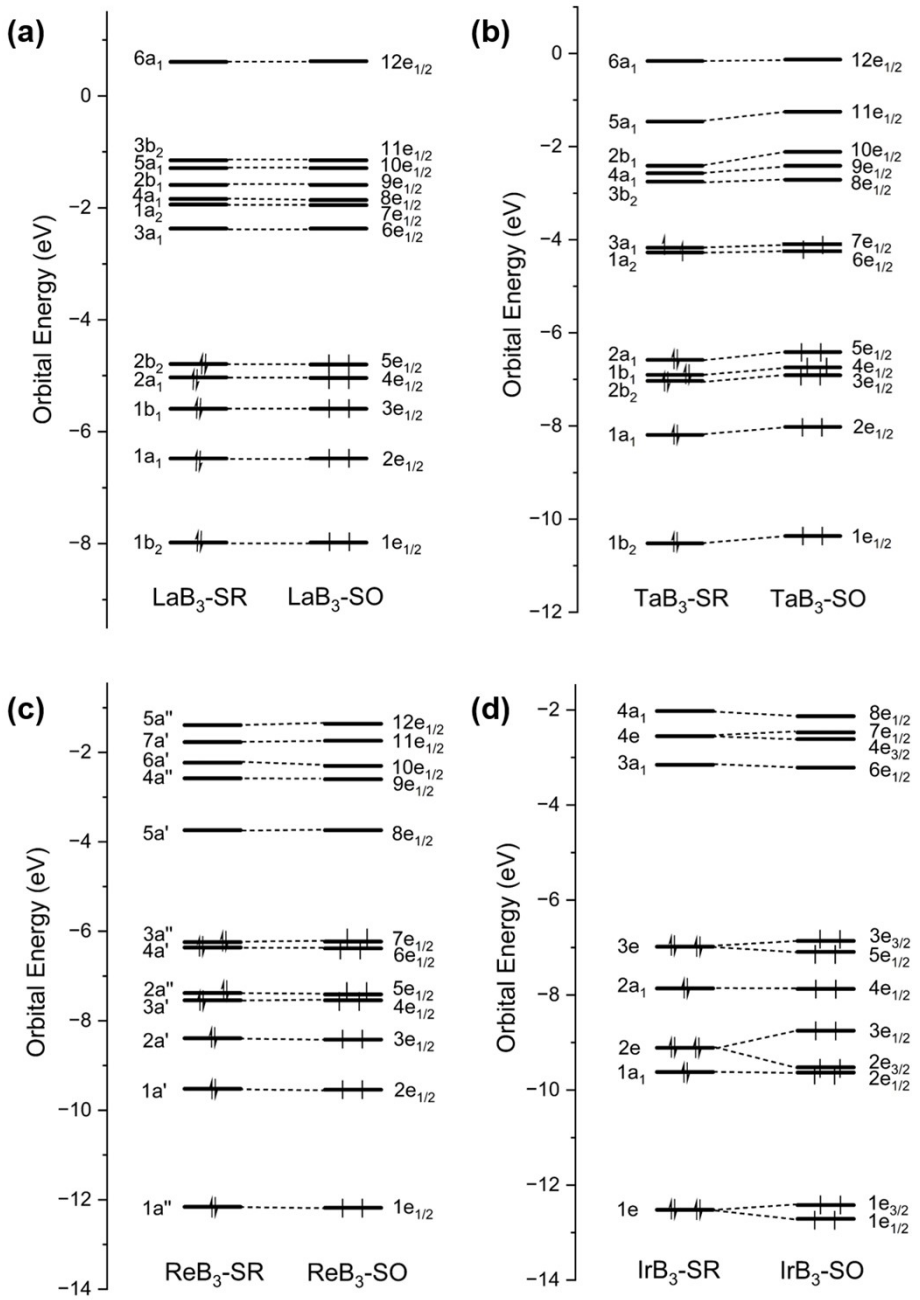

Fig. S11 Occupied and virtual Kohn-Sham molecular orbital energies (in eV) of the lowest-lying isomers for MB_3 (M = La, Ta, Re, Ir) (SR- and SO-ZORA/DFT/B3LYP).

Chemical Bonding Analysis.

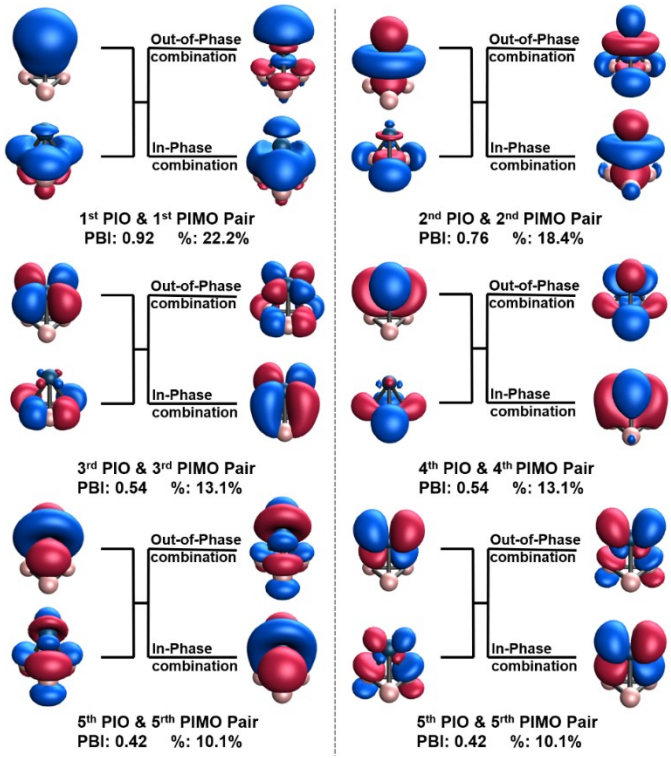

Fig. S12 Results of PIO analysis for the ground state of IrB_3 with Ir and B_3 as two neutral fragments. Six PIMO pairs and their relationship with PIO pairs are shown, with the PIO-based bond indices (abbreviated as PBI) and its contribution (as %) to the total interactions between two fragments given below each PIMO pair. The other minority of bonding interactions are not shown.

Table S7. QTAIM Local and Integral Properties corresponding to **Fig. 7** at the DFT/PBE Level: Electron Density ρ (in a.u.), Density Laplacian $\nabla^2\rho_b$ (in a.u.), Energy-Density H (in a.u.) and Bond Ellipticity ε for MB_3 (M = La, Ta, Re and Ir) Clusters. The Values for the Lowest-Lying Structures are Labeled in Bold Black Font.

Bond	BCP	ρ	$\nabla^2\rho_b$	H	ε
M-B	**LaB_3-C_{2v}**	**0.087**	**0.026**	**-0.047**	**0.16**
	LaB_3-C_{3v}	0.074	0.118	-0.027	0.00
	TaB_3-C_{2v}	**0.126**	**0.016**	**-0.090**	**0.29**
	TaB_3-C_{3v}	0.122	0.109	-0.077	2.27
	ReB_3-C_{2v}	0.157	-0.143	-0.162	0.20
	ReB_3-C_s	**0.164[a]/0.148[b]**	**-0.180[a]/-0.007[b]**	**-0.156[a]/-0.119[b]**	**0.62[a]/0.69[b]**
	IrB_3-C_{2v}	0.161	-0.180	-0.152	0.28
	IrB_3-C_{3v}	**0.157**	**-0.219**	**-0.150**	**0.06**
Bond	BCP	ρ	$\nabla^2\rho_b$	H	ε
B-B	B_4	0.167	-0.324	-0.173	0.46
	LaB_3-C_{2v}	**0.166**	**-0.324**	**-0.171**	**0.43**
	LaB_3-C_{3v}	0.154	-0.136	-0.139	2.31
	TaB_3-C_{2v}	**0.163**	**-0.332**	**-0.167**	**0.19**
	TaB_3-C_{3v}	0.134	-0.084	-0.108	0.70
	ReB_3-C_{2v}	0.162	-0.301	-0.132	0.510.15
	ReB_3-C_s	\	\	\	\
	IrB_3-C_{2v}	0.140	-0.196	-0.124	0.08
	IrB_3-C_{3v}	\	\	\	\

[a] For C_s-ReB_3, the QTAIM Properties of two equivalent Re-B bond

[b] For C_s-ReB_3, the QTAIM Properties of one longer Re-B bond

Structural Transformation of MB_3 Clusters along the 5d metals.

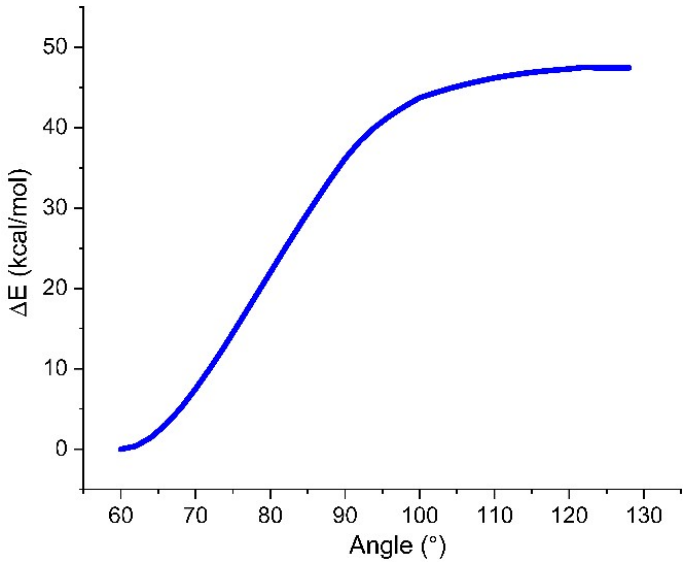

Fig. S13 LST curves for structural transformation process with respect to the angles between three boron atoms at the PBE/def2-SVP level. Note: the transformation direction from left to right represents the geometric change from C_{3v} to C_{2v} symmetries.

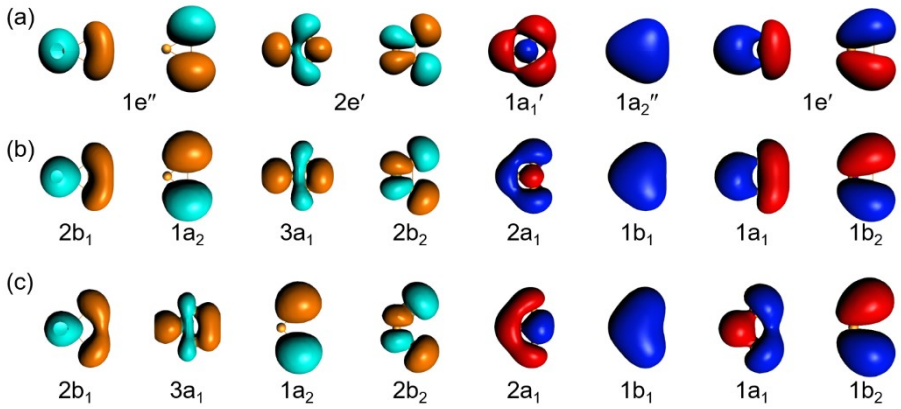

Fig. S14 Selected canonical molecular orbital (CMO) transition from the triangular B_3 to a ring-opened structure: **(a)-(c)** represents the canonical molecular orbitals of B_3 units related to geometries in IrB_3, LaB_3 and TaB_3 molecules, respectively.

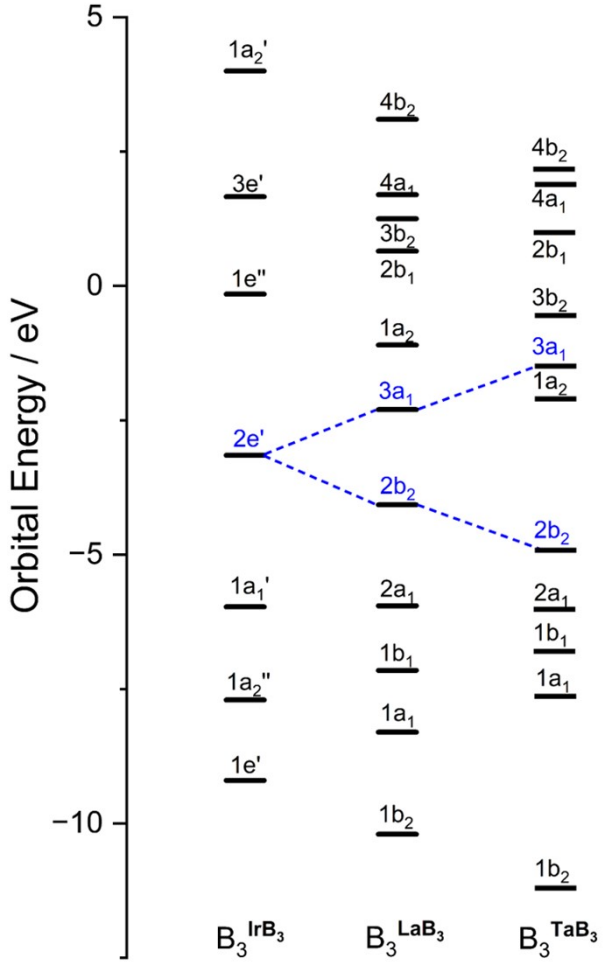

Fig. S15 The CMO energy levels from the triangular B_3 to a ring-opened structure, where the energy levels of the canonical molecular orbitals for B_3^{IrB3}-B_3^{TaB3} are obtained from single-point calculations of the B_3 units using their corresponding geometries in IrB_3, LaB_3 and TaB_3 molecules, respectively.

Table S8. Binding Energies (E, kcal/mol) of the 2D and 3D Geometries of MB_3 (M = La, Ta, Re, Ir) Molecules and Energy Changes (ΔE, kcal/mol) for 2D→3D transition at the B3LYP/TZ2P level.

Molecules	E(2D)	E(3D)	ΔE(2D→3D)
$^1LaB_3$	-402.43	-307.01	95.42
$^3TaB_3$	-466.66	-438.20	28.46
$^1ReB_3$	-502.59	-519.55	-16.96
$^1IrB_3$	-497.46	-511.93	-14.47

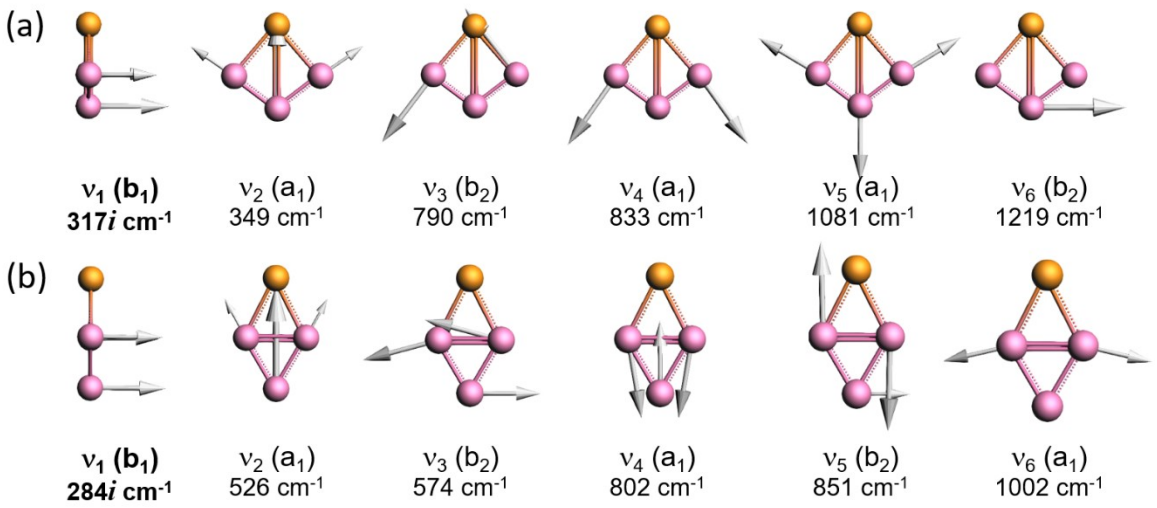

Fig. S16 Vibrational modes of the singlet 2D (C_{2v} symmetry) structures for **(a)** ReB_3 and **(b)** IrB_3 molecules.

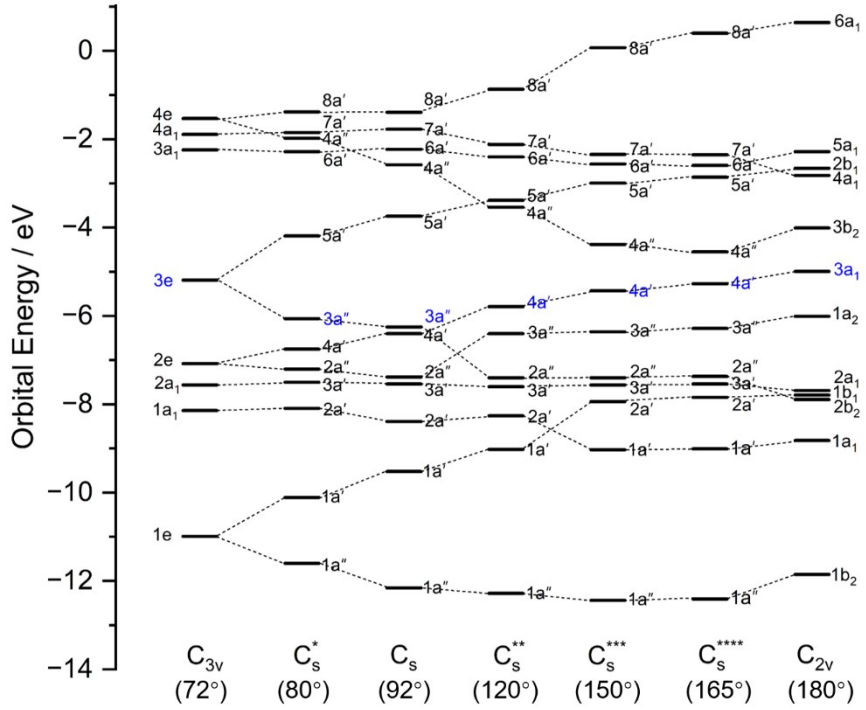

Fig. S17 The correlation of the CMOs for ReB_3 molecules with respect to the irreducible representations, as the reaction coordinate progresses from the 3D-C_{3v} triangular pyramid geometry (the 1st column) to the 3D-C_s structure (the 3rd column), and subsequently to the 2D-C_{2v} planar structure (the 7th column), by changing the dihedral angles (θ, in parentheses)

between metals and B_3 moieties. The HOMO is plotted in blue. The other structures along the transformation process are distinguished by a superscript asterisk.

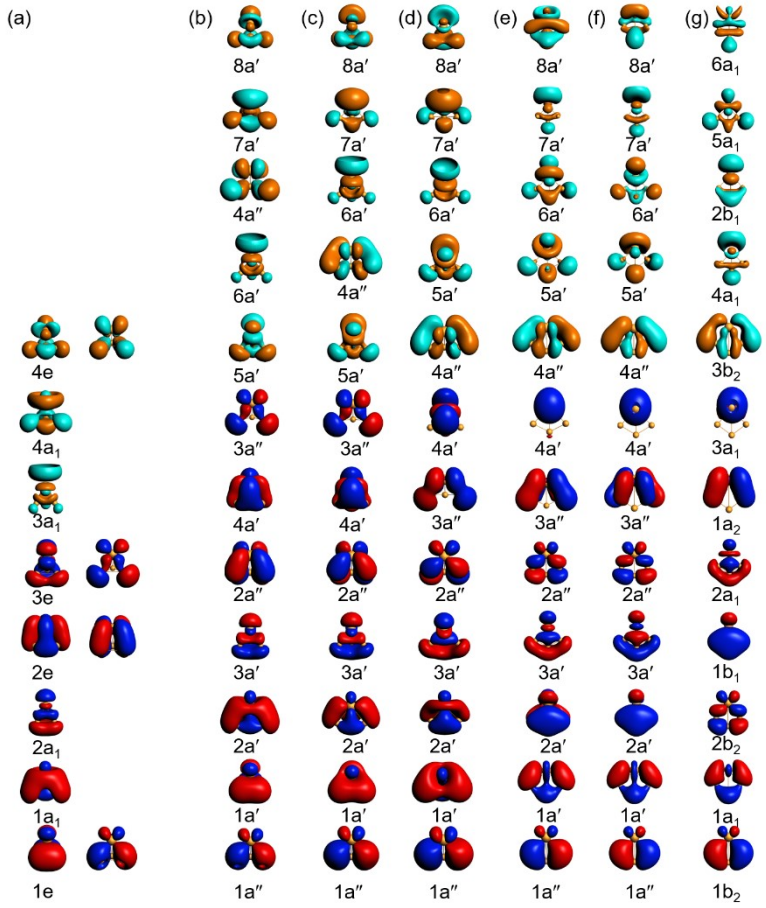

Fig. S18 The correlation of the CMOs with respect to the irreducible representation along the reaction coordinate, in which the energy levels of these orbitals are shown in Fig. S16.

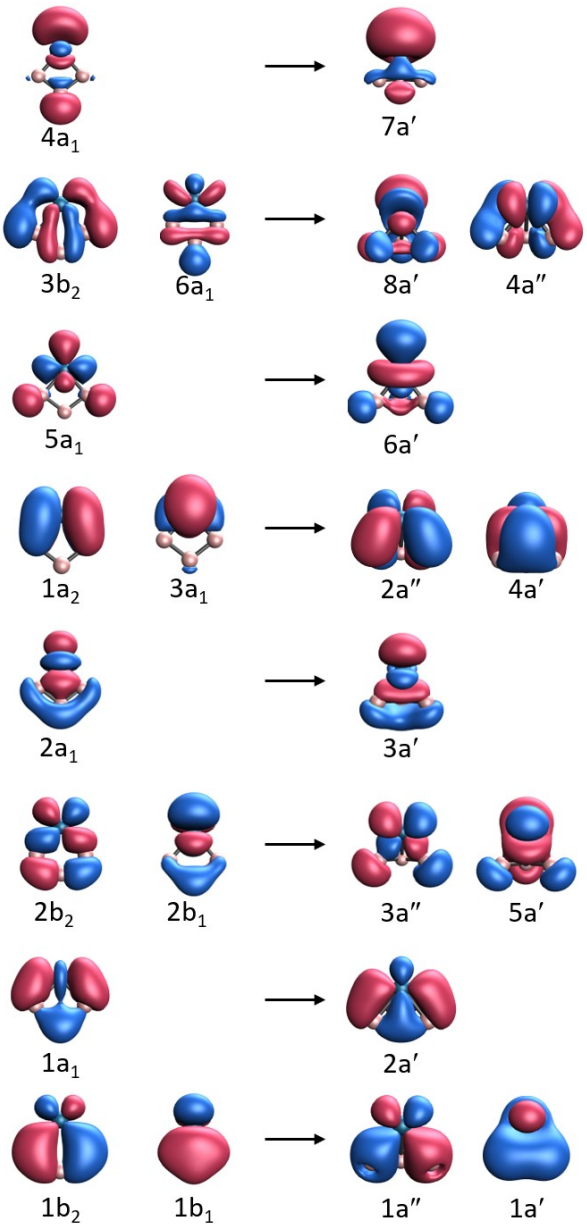

Fig. S19 The CMO correlation for the structural transformation of ReB_3 cluster from 2D (C_{2v} symmetry) to 3D (C_s symmetry), corresponding to the energy-level correlation in **Fig. 5a**.

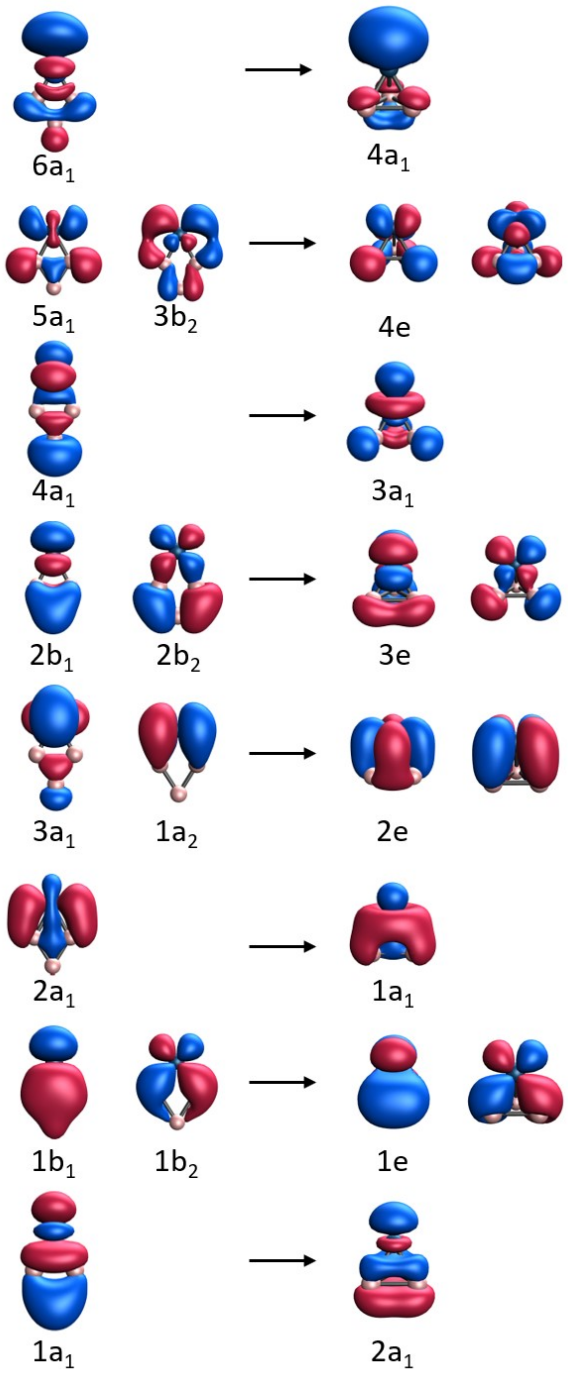

Fig. S20 The canonical molecular orbital correlation for the structural transformation of IrB_3 cluster from 2D (C_{2v} symmetry) to 3D (C_{3v} symmetry), corresponding to the energy-level correlation diagram in **Fig. 5b**.

Table S9. HOMO-LUMO Gap of the Isomers for MB_3 (M= La, Ta, Re, Ir) Clusters at the B3LYP Levels. The HOMO-LUMO Gaps for the Lowest-Lying Structures are Labeled in Bold Black Font.

M in MB_3	2D /eV	3D /eV
Re	0.98	**2.57**
Ir	1.32	**3.83**